Original Research

# A CT-based radiomics nomogram for differentiation of benign and malignant small renal masses (≤4 cm)

Shengxing Feng [a,b], Mancheng Gong [b,*], Dongsheng Zhou [a,b], Runqiang Yuan [b], Jie Kong [a,b], Feng Jiang [a,b], Lijie Zhang [a,b], Weitian Chen [a,b], Yueming Li [a,b]

[a] *The First Clinical School of Medicine, Guangdong Medical University, Zhanjiang, China*
[b] *Department of Urology, The People's Hospital of Zhongshan, Zhongshan, China*

A B S T R A C T

*Rationale and Objectives:* Based on radiomics signature and clinical data, to develop and verify a radiomics nomogram for preoperative distinguish between benign and malignant of small renal masses (SRM).
*Materials and Methods:* One hundred and fifty-six patients with malignant (n = 92) and benign (n = 64) SRM were divided into the following three categories: category A, typical angiomyolipoma (AML) with visible fat; category B, benign SRM without visible fat, including fat-poor angiomyolipoma (fp-AML), and other rare benign renal tumors; category C, malignant renal tumors. At the same time, one hundred and fifty-six patients included in the study were divided into the training set (n = 108) and test set (n = 48). Respectively from corticomedullary phase (CP), nephrogram phase (NP) and excretory phase (EP) CT images to extract the radiomics features, and the optimal features were screened to establish the logistic regression model and decision tree model, and computed the radiomics score (Rad-score). Demographics and CT findings were evaluated and statistically significant factors were selected to construct a clinical factors model. The radiomics nomogram was established by merging Rad-score and selected clinical factors. The Akaike information criterion (AIC) values and the area under the curve (AUC) were used to compare model discriminant performance, and decision curve analysis (DCA) was used to assess clinical usefulness.
*Results:* Seven, fifteen, nineteen, and seventeen distinguishing features were obtained in the CP, NP, EP, and three-phase joint, respectively, and the logistic regression and decision tree models were built based on this features. In the training set, the logistic regression model works better than the decision tree model for distinguishing categories A and B from category C, with the AUC of CP, NP, EP and three-phase joint were 0.868, 0.906, 0.937 and 0.975, respectively. The radiomics nomogram constructed based on the three-phase joint Rad-score and selected clinical factor performed well on the training set (AUC, 0.988; 95% CI, 0.974-1.000) for differentiation of categories A and B from category C. In the test set, the AUC of clinical factors model, radiomics signature and radiomics nomogram for discriminating categories A and B from category C were 0.814, 0.954 and 0.968, respectively; for the identification of category A from category C, the AUC of the three models were 0.789, 0.979, 0.985, respectively; for discriminating category B from category C, the AUC of the three models were 0.853, 0.915, 0.946, respectively. The radiomics nomogram had better discriminative than the clinical factors model in both training and test sets (*P* < 0.05). The radiomics nomogram (AIC = 40.222) with the lowest AIC value was considered the best model compared with that of the clinical factors model (AIC = 106.814) and the radiomics signature (AIC = 44.224). The DCA showed that the radiomics nomogram have better clinical utility than the clinical factors model and radiomics signature.
*Conclusions:* The logistic regression model has better discriminative performance than the decision tree model, and the radiomics nomogram based on Rad-score of three-phase joint and clinical factors has a good predictive

---

effect in differentiating benign from malignant of SRM, which may help clinicians develop accurate and individualized treatment strategies.

## Introduction

The small renal masses (SRM) are defined as the maximum size in abdominal imaging is 4 cm or less contrast enhanced mass [1]. With the continuous development and widespread application of advanced cross-sectional imaging, the number of detection of SRM has been increasing [2,3]. Previous study have shown that more than 50% of renal masses are incidental findings during routine imaging [4]. According to statistics, 48% to 66% of the renal tumors discovered in the examination were SRM and 38% of the removed renal tumors were SRM [1,5,6]. However, up to 25% of SRM are benign tumors [7], with renal AML being the most common. In addition, fp-AML is similar to renal cell carcinoma (RCC) in imaging characteristics because it lacks macroscopic fat, which makes it difficult to distinguish these lesions from RCC in conventional CT analysis, which is prone to misdiagnosis. Current guidelines believe that surgery remains the primary treatment modality for malignant renal tumors, while for benign renal tumors such as AML, active surveillance is the most appropriate option, especially for SRM [8]. Therefore, preoperative identification between benign and malignant of SRM is very necessary, which can reduce unnecessary excessive surgery and satisfy the current requirements for precise and individualized treatment.

As an emerging auxiliary and diagnostic technology, radiomics can improve the accuracy of tumor diagnosis and provide clinicians with more objective and quantitative auxiliary support through high-throughput, non-invasive extraction of lesion information and a deeper understanding of tumor heterogeneity [9,10]. Studies have shown that radiomics shows great potential in the field of oncology, such as predicting tumor type, distinguishing benign from malignant tumors, and tumor aggressiveness, among many other aspects [11,12]. In this study, we validated the value of the radiomics nomogram in preoperative diagnosis of benign and malignant of SRM.

## Materials and methods

### Patients

Retrospective analysis of 156 patients with SRM who underwent preoperative contrast-enhanced CT from January 2015 to April 2022, including 92 malignant tumors (79 clear cell renal cell carcinoma (ccRCC), 7 papillary renal carcinoma, 6 chromophobe renal carcinoma) and 64 benign tumors (25 fp-AML, 1 metanephricadenoma, 1 renal oncocytoma, 37 typical AML). The inclusion criteria of the research subjects are as follows: (1) Postoperatively diagnosed with renal tumor and with clear pathological classification; (2) Complete three-phase CT scan (CP, NP, EP) with good image quality, meeting the analysis requirements; (3) Renal tumors with maximal diameter ≤4 cm on CT: category A, typical AML with visible fat; category B, benign SRM without visible fat, including fp-AML, oncocytoma, and other rare benign renal tumors; category C, malignant renal tumors. Below were the criteria for exclusion: (1) Patients receiving interventions such as radiotherapy or chemotherapy therapy before surgery; (2) Image artifacts and overlaps lead to poor or damaged image quality and cannot be diagnosed.

### CT image acquisition

The CT scanning was acquired using 256-slice multidetector CT equipment (Brilliance, Philips Healthcare). The specific parameters: tube voltage 120-kVp, tube current variable, layer thickness was 3.0mm, layer spacing was 3.0mm, matrix 512×512. Eighty milliliters of nonionic contrast agent (Ioversol, Jiangsu Hengrui Medicine Co., Ltd., Nanjing, China) were administered into an antecubital vein at a dynamic rate of 3.3 ml/s. The CP, NP and EP were obtained at 30s, 65s, and 180s following the start of contrast injection, respectively.

### Drawing tumors and extracting features

All three-phase enhanced CT images were transferred from the picture archiving and communication system to 3D Slicer software (version: 4.10.2.) in DICOM format with original dimensions and resolution. The three-dimensional (3-D) regions of interest (ROI) were drawn along no more than 1mm of the lesion edge on CP, NP, and EP images. Fig. 1 showed an example of segmentation.

All CT images were resampled to a voxel size of $1 \times 1 \times 1$ mm and discretized to grayscale with the bandwidth set to 25 before extracting radiomics features. In total, 107 imaging features were extracted in each patient, including 14 shape features, 18 first order features and 75 texture features. Finally, 479 radiomics features were obtained using LoG (σ: 0.5, 1.0, 1.5, 2.0). For more information on radiomics capabilities, visit https://pyradiomics.readthedocs. io/en/latest/#.

The radiomics signature was evaluated by calculating inter-class and intra-class correlation coefficients (ICC) using 35 randomly selected CT images (15 benign tumors and 20 malignant tumors). Reader 1 and reader 2 delineate the ROI respectively. The same procedure was repeated by reader 1 two weeks later to assess the consistency and stability of the extracted features. When the ICC is greater than 0.75, it was considered to be in good agreement. Reader 1 segmented the remaining images.

### Selecting features and creating radiomics signature

A ratio of 7:3 was used to randomly divide the acquired characteristics of patients into the training set (n = 108) and the test set (n = 48). Before feature selection, z-score normalization was performed to remove the unit limits of the data. Further analysis focused on stable and reproducible radiomics features with ICC greater than 0.75. One-way analysis of variance (ANOVA) and least absolute shrinkage and selection operator (LASSO) were used to select the optimal features and eliminate irrelevant or redundant features through tenfold cross-validation. Using the selected features, the decision tree and logistic regression prediction models were constructed respectively, and the generalization of the models were verified in the independent test set. Rad-score was computed per patient, weighted by the LASSO coefficient for each patient. The discriminative effect of each model was evaluated by receiver operating characteristic (ROC) curve and AUC, and specificity, sensitivity and accuracy were also computed.

### Developing clinical factor model

Univariate analysis and multivariate logistic regression were used to test the significant differences of clinical factors between the two groups, and the clinical factors model was established.

### Radiomics nomogram construction and model performance evaluation

The radiomics nomogram was constructed in the training set by multiple logistic regression, incorporating statistically significant clinical factors and Rad-score of the best radiomics signature. The Hosmer and Lemeshow test was used to measure the goodness of fit of the model, and the correction curve was drawn. The AUC of the training set and test set were computed to evaluate the diagnostic efficacy of the radiomics

nomogram, radiomics signature, and clinical factors model, while specificity, sensitivity, and accuracy were also computed. The Akaike information criterion (AIC) value was used to measure the goodness of the model fit. DCA was used to evaluate the clinical benefit of nomogram in differentiating benign from malignant of SRM.

### Statistical analysis

Data analysis R software, version 4.2.0 was used for statistical analysis. Comparison of clinical factors between groups was done using univariate analysis. The Fisher's exact test or Chi-square test was employed to compare the qualitative data, while the t-test or Mann-Whitney U test was used to compare quantitative data. The development and calibration plots of the nomogram using the "rms" package, and the "generalhoslem" package is used to carry out the Hosmer-Lemeshow test. We performed LASSO regression model analysis with "glmnet" package. We plotted ROC curves with the "pROC" package. The Delong test was used to estimate the difference of AUC values between three models. We performed the DCA with the package "dca.R.". The level of statistical significance was set at $P < 0.05$.

### Results

#### Patients with clinical factors and clinical factors model building

A total of 156 patients were enrolled in this study, including 37 typical AML with visible fat (category A), 27 benign SRM without visible fat (category B), and 92 malignant SRM (category C), and the mean age of categories A, B, and C masses were 43.89±11.12 years, 45.00±12.54 years and 54.64±12.12 years, respectively; the average sizes were 28.73 ±8.41 mm, 21.91±8.15 mm and 31.19 ±8.04 mm, respectively. The clinical features of benign SRM (categories A+B) and malignant SRM (category C) were shown in Table 1. As shown in Table 2, the univariate and multivariate logistic regression found that male sex, larger tumor, and older age were significant risk indicators for malignancy. Tumor location, height, weight and BMI were not statistically significant between groups.

#### Radiomics feature analysis and model construction

Of the 420, 396 and 310 radiomics features with good agreement were obtained in CP, NP and EP CT images, respectively, with ICC from 0.750 to 1.000. After one-way ANOVA and LASSO logistic regression, the features dimensionality reduction was performed (Fig. 2), and 7, 19, 15, and 17 most valuable radiomics features were obtained in the CP, NP, EP, and three-phase joint, respectively. Finally, logistic regression and decision tree models were constructed, ROC curve was drawn and AUC value, specificity, sensitivity and accuracy were computed. In the training set, the logistic regression model works better than the decision tree model for distinguishing categories A and B from category C, with the AUC of CP, NP, EP and three-phase joint were 0.868, 0.906, 0.937 and 0.975, respectively (Supplementary Table 1). The following is the formula for calculating Rad-score:

Rad-score=13.562-0.878*A-0.063*B+0.056*C+1.149*D-0.543*E-0.824*F+0.668*G-10.335*H-0.240*I+0.454*J+0.516*K-1.845*L-0.468*M-1.019*N-0.076*O+1.352*P+0.264*Q. The A to Q indicate the significant radiomics features of the three-phase joint, as shown in Supplementary Table 2. And the radiomics signature was established based on the Rad-score of three-phase joint.

#### Construction of radiomics nomogram and performance evaluation of three models

Radiomics nomogram was developed by multivariable logistic regression using clinical factors (age, sex, and tumor size) and Rad-score of three-phase joint (Fig. 3a). In the calibration curve and Hosmer-Lemeshow test, both the training ($P = 0.998$) and test ($P = 0.921$) sets were well calibrated (Fig. 3b, c).

Table 3 shows the diagnostic efficacy of the three models (clinical factors model, radiomics signature, and radiomics nomogram) in differentiating benign (categories A and B) from malignant (category C) of SRM in training (AUC = 0.852, 0.975, 0.88) and test (AUC = 0.814,
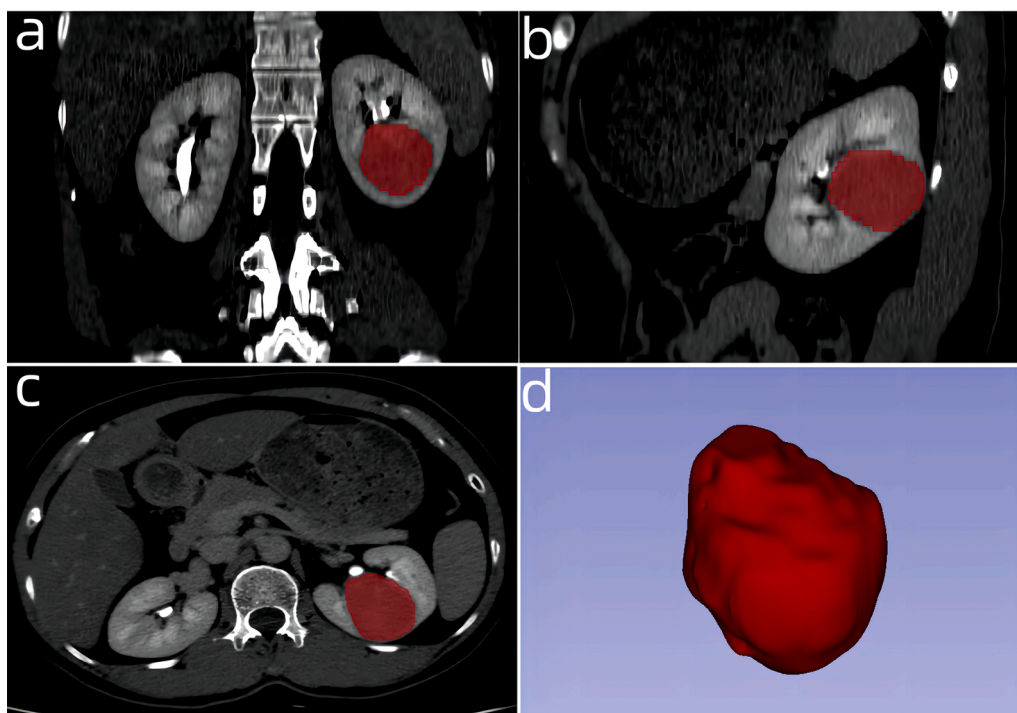


**Fig. 1.** Tumor segmentation in three dimensions manually. (a) Segmentation on the coronal section. (b) Segmentation on the sagittal section. (c) Segmentation on the transverse section. (d) Three-dimensional volumetric reconstruction.

**Table 1**

Clinical factors of benign and malignant small renal masses.

| Clinical factor | Age(year) | Gender (male/female) | Tumor size (mm) | Location(left/right) | Height(cm) | Weight(kg) | BMI(kg/m$^2$) |
| --- | --- | --- | --- | --- | --- | --- | --- |
| Malignant renal tumor(n=92) | 54.65 ± 12.12 | 57/35 | 31.19 ± 8.04 | 44/48 | 164.49 ±8.19 | 64.75 ±11.20 | 23.83 ±3.18 |
| Benign renal tumor(n=64) | 44.36 ± 11.66 | 13/51 | 25.85 ± 8.91 | 37/27 | 160.47 ±7.07 | 60.53 ±11.45 | 23.59 ±4.11 |
| t/X2 | 5.301 | 24.804 | - | 1.134 | 3.188 | 2.294 | 0.400 |
| P | <0.001 | <0.001 | <0.001 | 0.287 | 0.002 | 0.023 | 0.690 |

**Table 2**

Univariate and multivariate logistic regression analysis of the clinical factors.

| Characteristics | Univariate analysis | | | Multivariate analysis | | |
| --- | --- | --- | --- | --- | --- | --- |
| | OR | 95% CI | P | OR | 95% CI | P |
| Gender(male/ female) | 8.679 | 3.404-25.507 | <0.0001 | 9.188 | 3.174-31.206 | 0.0001 |
| Age | 0.934 | 0.899-0.965 | 0.0001 | 0.937 | 0.898-0.973 | 0.0013 |
| Tumor size | 0.920 | 0.876-0.963 | 0.0005 | 0.912 | 0.857-0.965 | 0.0021 |
| Location(left/ right) | 0.809 | 0.371-1.748 | 0.5906 | | | |
| Height | 0.920 | 0.871-0.967 | 0.0017 | 0.974 | 0.878-1.080 | 0.6196 |
| Weight | 0.957 | 0.923-0.990 | 0.0143 | 0.989 | 0.937-1.044 | 0.6911 |
| BMI | 0.948 | 0.846-1.058 | 0.3498 | | | |

CI, confidence interval;OR, odds ratio.

0.954, 0.968) sets. The ROC curves for the three models in the training and test sets were shown in Supplementary Fig. 1 and Supplementary Fig. 2. The radiomics nomogram had better discriminative than the clinical factors model in both training and test sets ($P = 0.0007, 0.0258$). Compared with the clinical factors model, the radiomics signature AUC was better ($P = 0.0008$) in the training set, while the radiomics signature was not significantly different from the clinical factors model in the test set ($P = 0.0546$). In the training and test sets, the AUC of the radiomics nomogram and the radiomics signature were not significantly different ($P = 0.1259, 0.1278$). The following is the formula for calculating Nomo-score:

Nomo-score=4.2187+0.8774*Rad-score+1.7101*gender-0.0849*age-0.0561*size

Table 4 shown the diagnostic performance of the three models in the test set between categories A and C, and between categories B and C. The AUC were 0.789, 0.979, 0.985 and 0.853, 0.915, 0.946, respectively. Supplementary Fig. 3 and Supplementary Fig. 4 shows the ROC curves of the three models. For the identification of categories A and C, compared with the clinical factors model, the radiomics nomogram ($P = 0.0082$) and radiomics signature ($P = 0.0115$) had better AUC values, but the AUC of the radiomics signature and the nomogram were not significantly different ($P = 0.3013$). The radiomics nomogram showed the highest AUC value for the differentiation between categories B and C, but no significant differences were observed between the three models ($P > 0.05$).

The radiomics nomogram (AIC = 40.222) with the lowest AIC value was considered the best model compared with that of the clinical factors model (AIC = 106.814) and the radiomics signature (AIC = 44.224). The decision curve of the three models were shown in Fig. 4. The DCA indicated that radiomics nomograms have better clinical utility than clinical factors model and radiomics signatures in distinguishing benign from malignant of SRM.

## Discussion

Differentiating benign from malignant preoperatively is of great clinical significance due to the vast differences in treatment
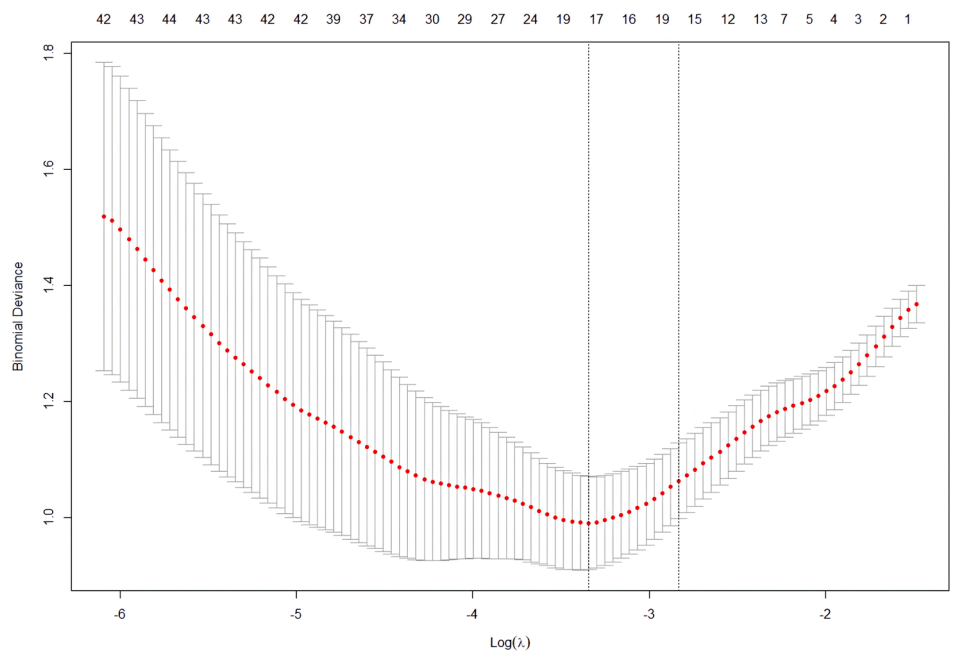


**Fig. 2.** Radiomics features of three-phase joint were selected using the LASSO regression model. A tenfold cross-validation procedure was used for tuning parameter (λ) in the LASSO model according to the minimum error criterion. The optimal value of LASSO tuning parameter (λ) is represented by the vertical dashed line, and 0.035 was chosen as the optimal value.
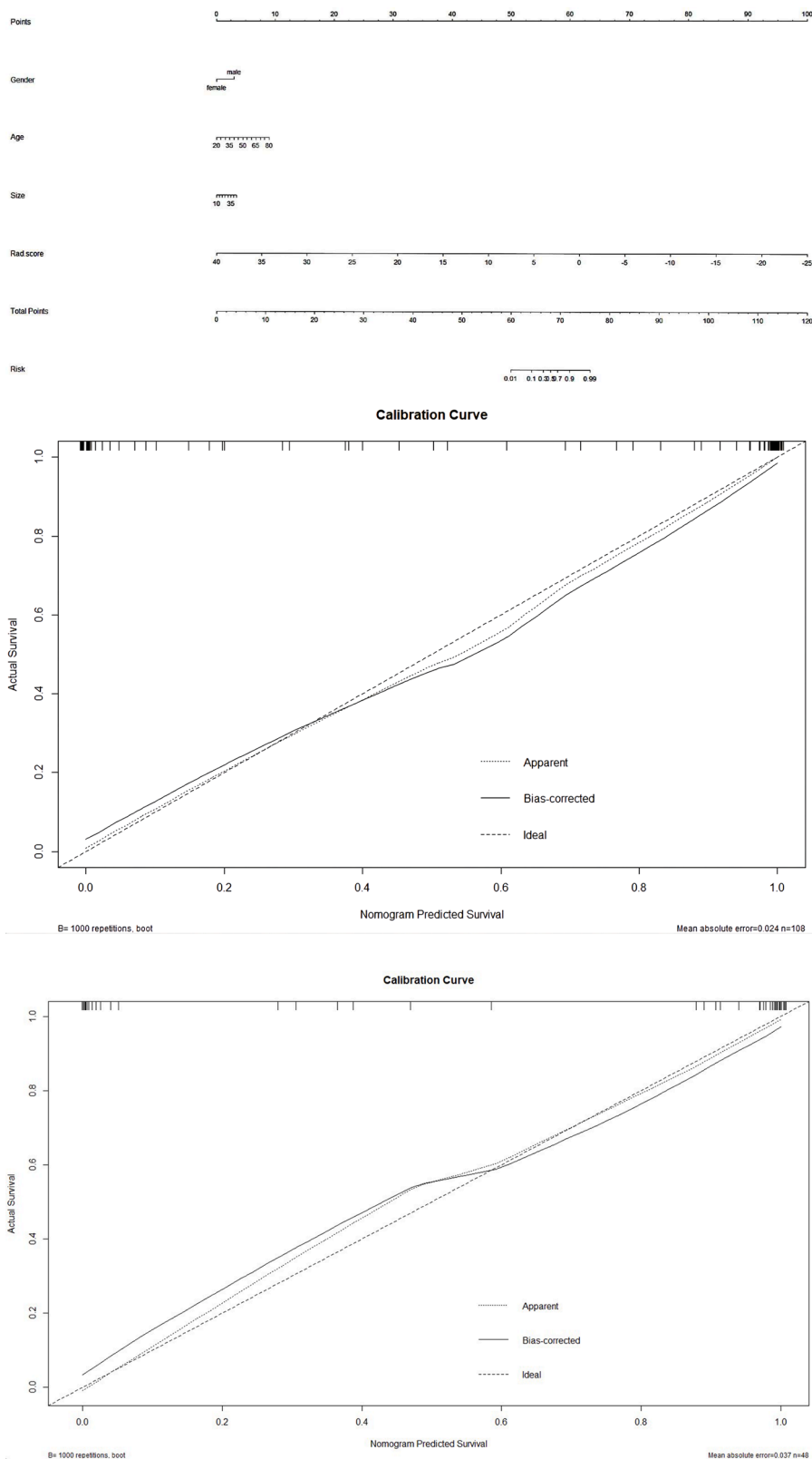
**Fig. 3.** The radiomics nomogram and calibration curves. (a) The radiomics nomogram is through a combination of gender, tumor size, age and Rad-score. Calibration curves of the nomogram in the training (b) and test (c) sets. The 45° straight line indicates the ideal prediction. The closer the two curves are, the higher the accuracy.

requirements, biologic characteristics, and prognosis between the two tumors. The imaging features of fp-AML without obvious necrosis and hemorrhage are similar to renal cancer, and the differential diagnosis by conventional imaging is difficult, especially when the tumor is smaller than 4 cm [13]. In this study, logistic regression model, decision tree model, and clinical factors model were constructed by selecting the optimal radiomics features and statistically significant clinical factors. The results indicated that the logistic regression model had better

**Table 3**

Diagnostic performance of three models for benign (categories A and B) and malignant (categories C) masses.

| Model | Training set(n=108) | | | | Test set(n=48) | | | |
|---|---|---|---|---|---|---|---|---|
| | AUC(95% CI) | Sensitivity | Specificity | Accuracy | AUC(95% CI) | Sensitivity | Specificity | Accuracy |
| Clinical factor model | 0.852(0.782, 0.923) | 0.682 | 0.844 | 0.778 | 0.814(0.690, 0.938) | 0.450 | 0.857 | 0.688 |
| Radiomics signature | 0.975(0.954, 0.997) | 0.886 | 0.922 | 0.907 | 0.954(0.902, 1.000) | 0.900 | 0.857 | 0.875 |
| Radiomics nomogram | 0.988(0.974, 1.000) | 0.909 | 0.938 | 0.926 | 0.968(0.928, 1.000) | 0.900 | 0.893 | 0.886 |

CI, confidence interval

**Table 4**

Diagnostic performance of the three models in the test set between categories A and categories C and categories B and categories C.

| Model | Categories A and C Test set(n=40) | | | | Categories B and C Test set(n=36) | | | |
|---|---|---|---|---|---|---|---|---|
| | AUC(95% CI) | Sensitivity | Specificity | Accuracy | AUC(95% CI) | Sensitivity | Specificity | Accuracy |
| Clinical factor model | 0.789(0.648, 0.929) | 0.333 | 0.857 | 0.700 | 0.853(0.727, 0.978) | 0.625 | 0.857 | 0.806 |
| Radiomics signature | 0.979(0.954, 0.997) | 0.917 | 0.857 | 0.875 | 0.915(0.823, 1.000) | 0.875 | 0.857 | 0.861 |
| Radiomics nomogram | 0.985(0.957, 1.000) | 0.917 | 0.893 | 0.900 | 0.946(0.878, 1.000) | 0.750 | 0.893 | 0.861 |

CI, confidence interval.
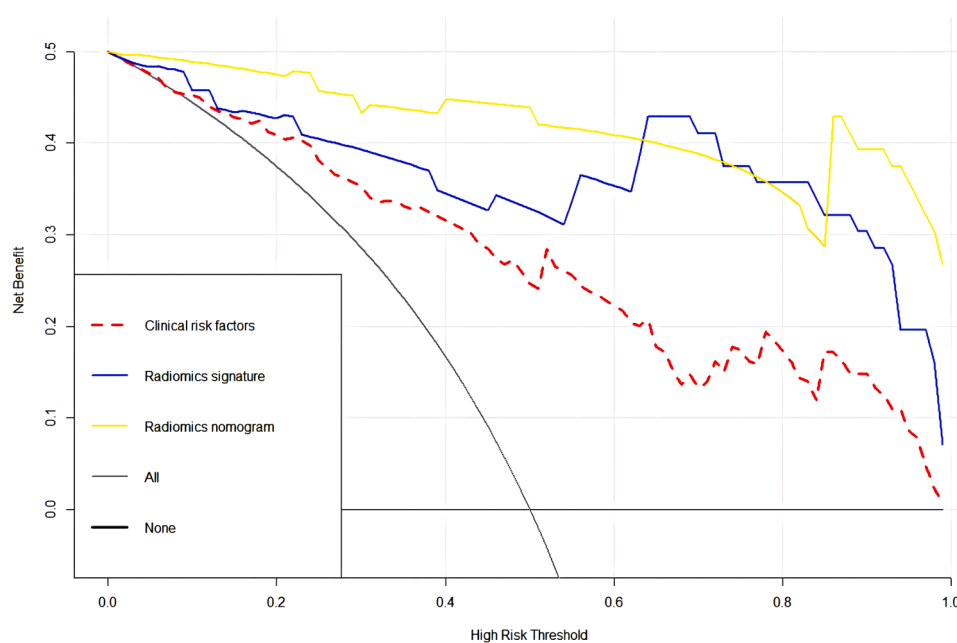


**Fig. 4.** An analysis of decision curves for three models, with the y-axis representing the net benefit and the x-axis representing the threshold probability. The yellow, blue and red lines reflect the net benefit of the radiomics nomogram, the radiomics signature and the clinical factors model, respectively.

discriminative performance, and the three-stage combined model had the best effect. Radiomics nomogram based on Rad-score and selected clinical factors has good predictive value and clinical benefits in differentiating benign from malignant of SRM.

CT is one of the most important and most widely used methods of SRM diagnosis in current imaging examinations [14]. Various strategies have been proposed to obtain conventional CT imaging features to distinguish benign from malignant. Xie et al. analyzed 329 patients with SRM by constructing a nomogram, and the regression model results showed that tumor size and tumor CT profile were predictors of SRM histopathological subtypes. After external verification, the C-index is 0.887 [15]. Yang et al. collected 33 fp-AML and 54 ccRCC patients, multivariate analysis shown that the hypodense rim, angular interfaces, high unenhanced attenuation, and homogeneous enhancement patterns may be specific CT features of fp-AML [16]. Choi et al. studied the four-phase CT imaging features of 84 patients with SRM and the results suggested that the degree of CP enhancement is the most valuable parameter to characterize of SRM [17].

Radiomics has been developed recently to identify subtle changes in

CT images that cannot be detected visually, providing more objective diagnostic information. Compared with traditional CT to qualitatively evaluate the size and enhancement degree of tumor lesions, radiomics can obtain quantitative and high-throughput features from images, comprehensively analyze the entire tumor ROI, and assist decision-making more scientifically and accurately [18,19]. Several studies have demonstrated that radiomics can be used to distinguish benign from malignant renal tumors. You et al. performed quantitative texture analysis on phase 4 CT enhanced images of renal tumors, and selected five texture features with significant discriminative ability for the discrimination between fp-AML and ccRCC, with the AUC of 0.850 [20]. Feng et al. performed texture analysis on phase 3 CT enhanced images of 58 patients, and used support vector machine to establish a classification model to distinguish RCC from fp-AML, with the AUC of 0.955 [21]. Li et al. included 122 patients with renal tumors to establish a radiomics nomogram for distinguishing oncocytoma from ccRCC, the AUC in the training and test sets were 0.960 and 0.898 [22]. Yap et al. analyzed 735 patients with CT radiomics features based on shape and texture to differentiate benign form malignant renal tumors, and the results

showed that shape features also have similar discriminative power to texture features [23]. Erdim et al. Selected two-dimensional cross-sections for texture analysis to identify between benign and malignant of renal tumors. Among the eight machine learning classifiers, the random forest model showed the best ability to discriminate the features of cortical enhanced CT images [24]. Uhlig et al. included 91 patients with renal tumors, and based on parenchymal enhanced CT features only, the results showed that radiomics features were more accurate in differentiating renal tumors than radiologists [25].

There are numerous differences and improvements between our study and the radiomics studies described above. First, we mainly studied renal masses ≤4 cm in diameter. Compared with larger kidney cancers, which are prone to necrosis and marked enhancement, the SRM are small, slow-growing, and lacks characteristics on conventional CT and MRI images. Therefore, the efficient identification of SRM are more clinically meaningful than the identification between large renal tumors. Second, most previous studies have used the largest cross-section to extract features. The 3-D ROI was used in this study. Compared with two-dimensional ROI, 3-D analysis is more reliable and comprehensive, allowing us to uncover the imaging features of tumors and better understand their heterogeneity [26]. Third, we divided the included patients into three categories, and constructed a logistic regression model, a decision tree model, a clinical factor model, and a radiomics nomogram. Radiomics nomogram has better predictive ability for distinguishing categories A, B and C, categories A and C, and categories B and C, and has a higher accuracy than traditional CT [27,28]. Fourth, this study included age, gender, and tumor size, and found that males, older age, and larger tumors were more likely to be malignant lesions, while gender was a stronger predictor, consistent with Li and other studies [29–31].

In our study, several limitations were identified: First, our study used retrospective data for analysis. We only analyzed three-phase contrast-enhanced CT and did not include the plain scan phase. MRI imaging may lead to higher levels of evidence in the future. Second, samples were derived from one institute only. Prospective studies involving multiple centers and diversity are needed. Third, the number of different types is unbalanced, no subgroup analysis was performed, and further study with larger number of cases is needed. Fourth, we exclude those cases in which the surgery were not performed, potentially creating a selection bias.

## Conclusion

In this study, the logistic regression and decision tree models based on radiomics optimal features can accurately distinguish benign from malignant of SRM, but the radiomics nomogram based on Rad-score of three-phase joint and selected clinical factors has higher accuracy and better clinical net or benefit. Radiomics nomogram can provide important support for clinical decision making and meet our current needs for accurate diagnosis and treatment of SRM.

## Ethical approval

Institutional Review Board approval was obtained.

## Informed consent

The requirement for informed consent was waived due to the retrospective nature of the study.

## Consent for publication

All authors consent to publication. No other consents were required or sought.

## CRediT authorship contribution statement

**Shengxing Feng:** Data curation, Writing – original draft, Conceptualization, Methodology, Software. **Mancheng Gong:** Supervision. **Dongsheng Zhou:** Visualization, Investigation. **Runqiang Yuan:** Writing – review & editing. **Jie Kong:** Conceptualization, Methodology, Software. **Feng Jiang:** Data curation, Writing – original draft. **Lijie Zhang:** Software, Validation. **Weitian Chen:** Software, Validation. **Yueming Li:** Writing – review & editing.

## Declaration of competing Interest

There is no conflict of interest. This research did not receive any specific grant from funding agencies in the public, commercial, or not-for-profit sectors.

## Supplementary materials

Supplementary material associated with this article can be found, in the online version, at doi:10.1016/j.tranon.2023.101627.

## References

[1] IS Gill, M Aron, DA Gervais, et al., Clinical practice. small renal mass, N. Engl. J. Med. (7) (2010) 624–634.
[2] HG Welch, JS Skinner, FR Schroeck, et al., Regional variation of computed tomographic imaging in the United States and the risk of nephrectomy, Jama Int. Med. (2) (2018) 221–227.
[3] L Bukavina, K Bensalah, F Bray, et al., Epidemiology of renal cell carcinoma: 2022 update, Eur. Urol. (2022).
[4] S Campbell, RG Uzzo, ME Allaf, et al., Renal mass and localized renal cancer: Aua guideline, J. Urol. (3) (2017) 520–529.
[5] MM Nguyen, IS Gill, LM. Ellison, The evolving presentation of renal carcinoma in the United States: trends from the surveillance, epidemiology, and end results program, J. Urol. (6) (2006) 2397–2400.
[6] CT Lee, J Katz, W Shi, et al., Surgical management of renal tumors 4 cm. or less in a contemporary cohort, J. Urol. 163 (3) (2000) 730–736.
[7] A Finelli, N Ismaila, B Bro, et al., Management of small renal masses: American Society of Clinical Oncology Clinical Practice Guideline, J. Clin. Oncol. (6) (2017) 668–680.
[8] B Ljungberg, L Albiges, Y Abu-ghanem, et al., European Association of Urology guidelines on renal cell carcinoma, Eur. Urol. (2020).
[9] Y Huang, C Liang, L He, et al., Development and validation of a radiomics nomogram for preoperative prediction of lymph node metastasis in colorectal cancer, J. Clin. Oncol. (18) (2016) 2157–2164.
[10] HJWL Aerts, ER Velazquez, RTH Leijenaar, et al., Decoding tumour phenotype by noninvasive imaging using a quantitative radiomics approach, Nat. Commun. 5 (2014) 4006.
[11] TP Coroller, P Grossmann, Y Hou, et al., Ct-based radiomic signature predicts distant metastasis in lung adenocarcinoma, Radiother. Oncol. 114 (3) (2015) 345–350.
[12] L Liang, X Zhi, Y Sun, et al., A nomogram based on a multiparametric ultrasound radiomics model for discrimination between malignant and benign prostate lesions, Front. Oncol. 11 (2021), 610785.
[13] P Nie, G Yang, Z Wang, et al., A Ct-based radiomics nomogram for differentiation of renal angiomyolipoma without visible fat from homogeneous clear cell renal cell carcinoma, Eur. Radiol. 30 (2) (2020) 1274–1284.
[14] S Wei, C Xu, Q Zhang, et al., Contrast-enhanced ultrasound for differentiating benign from malignant solid small renal masses: comparison with contrast-enhanced CT, Abdom. Radiol. (NY) (8) (2017) 2135–2145.
[15] H Xie, G Li, K Liu, et al., Development and validation of ct imaging-based preoperative nomogram in the prediction of unfavorable high-grade small renal masses, Cancer Manag. Res. (2019) 8731–8741.
[16] C Yang, S Shen, Y Chang, et al., Are there useful ct features to differentiate renal cell carcinoma from lipid-poor renal angiomyolipoma? AJR Am. J. Roentgenol. (5) (2013) 1017–1028.
[17] S Choi, SH Jeon, S. Chang, Characterization of small renal masses less than 4 cm with quadriphasic multidetector helical computed tomography: differentiation of benign and malignant lesions, Korean J. Urol. (3) (2012) 159–164.
[18] RJ Gillies, PE Kinahan, H. Hricak, Radiomics: images are more than pictures, they are data, Radiology (2) (2016) 563–577.
[19] V Kumar, Y Gu, S Basu, et al., Radiomics: the process and the challenges, Magn. Reson. Imaging 30 (9) (2012) 1234–1248.
[20] M You, N Kim, HJ. Choi, The value of quantitative ct texture analysis in differentiation of angiomyolipoma without visible fat from clear cell renal cell carcinoma on four-phase contrast-enhanced ct images, Clin. Radiol. (7) (2019) 547–554.

[21] Z Feng, P Rong, P Cao, et al., Machine learning-based quantitative texture analysis of CT images of small renal masses: differentiation of angiomyolipoma without visible fat from renal cell carcinoma, Eur. Radiol. (4) (2017) 1625–1633.

[22] X Li, Q Ma, C Tao, et al., A CT-based radiomics nomogram for differentiation of small masses (&lt; 4 cm) of renal oncocytoma from clear cell renal cell carcinoma, Abdom. Radiol. (NY) (11) (2021) 5240–5249.

[23] FY Yap, BA Varghese, SY Cen, et al., Shape and texture-based radiomics signature on ct effectively discriminates benign from malignant renal masses, Eur. Radiol. 31 (2) (2021) 1011–1021.

[24] C Erdim, AH Yardimci, CT Bektas, et al., Prediction of benign and malignant solid renal masses: machine learning-based CT texture analysis, Acad. Radiol. 27 (10) (2020) 1422–1429.

[25] J Uhlig, L Biggemann, MM Nietert, et al., Discriminating malignant and benign clinical T1 renal masses on computed tomography: a pragmatic radiomics and machine learning approach, Medicine 99 (16) (2020) 19725.

[26] F Ng, R Kozarski, B Ganeshan, et al., Assessment of tumor heterogeneity by CT texture analysis: can the largest cross-sectional area be used as an alternative to whole tumor analysis? Eur. J. Radiol. (2) (2012) 342–348.

[27] L Fang, K Bai, Y Chen, et al., A comparative study of contrast-enhanced ultrasound and contrast-enhanced ct for the detection and characterization of renal masses, Biosci. Trends (1) (2021) 24–32.

[28] S Wei, C Xu, Q Zhang, et al., Contrast-enhanced ultrasound for differentiating benign from malignant solid small renal masses: comparison with contrast-enhanced CT, Abdom. Radiol. (8) (2017) 2135–2145 (new York).

[29] C Li, G Qiao, J Li, et al., An ultrasonic-based radiomics nomogram for distinguishing between benign and malignant solid renal masses, Front. Oncol. (2022), 847805.

[30] A Kutikov, MC Smaldone, BL Egleston, et al., Anatomic features of enhancing renal masses predict malignant and high-grade pathology: a preoperative nomogram using the renal nephrometry score, Eur. Urol. (2) (2011) 241–248.

[31] Pierorazio PM, Johnson MH, Patel HD, et al. Management of renal masses and localized renal cancer: systematic review and meta-analysis. Ahrq Publication 16-ehc001-ef, 2016 167.